

Structural and optical properties of zinc sulphide nanoparticles synthesized via solid state reaction method

M. Jothibas¹ · S. Johnson Jeyakumar¹ · C. Manoharan² · I. Kartharinal Punithavathy¹ · P. Praveen³ · J. Prince Richard¹

Received: 29 July 2016 / Accepted: 26 September 2016 / Published online: 7 October 2016
© Springer Science+Business Media New York 2016

Abstract Pure Zinc sulfide nanoparticles were synthesized by an inexpensive Solid state reaction method using zinc acetate and thiourea at different temperatures (250–450 °C). The structural, functional, optical and morphological properties were characterized by using X-ray diffraction (XRD) analysis, Fourier transform infrared (FTIR) spectroscopy, UV–Vis spectroscopy, Photoluminescence (PL) spectroscopy and Scanning electron microscopy (SEM) with Energy dispersive X-ray analysis. XRD patterns confirmed the crystalline nature and cubic structure of the prepared products. Crystallite size, microstrain and dislocation density were also evaluated from the XRD data. The functional groups present in the samples were investigated by FTIR study. A blue shift in the absorption edges was noticed in the UV–Vis spectra. The PL spectra showed three emission peaks corresponding to both UV and visible emissions. SEM revealed the abundance of spherical shaped particles and the elements Zn and S alone are identified from EDS.

1 Introduction

In the recent days, semiconductor nanostructured materials have attracted a great interest due to their unique properties which are different from the bulk materials [1]. Mostly, one dimensional nanostructures have been prepared from II to VI and III to V group semiconductor materials. Among these ZnS, is a typical II–VI semiconductor compound with band gap energy of 3.6 eV and a small Bohr radius (2.4 nm) which make it an excellent candidate for exploring the intrinsic recombination processes in dense excitonic systems. ZnS is an important inorganic material for a variety of applications including optical coatings, solid-state solar cell windows, electro-optic modulators, photoconductors, field effect transistors, sensors, transductions' and light-emitting applications [2]. Several techniques have been employed to synthesize undoped ZnS nanoparticles: like Chemical vapor deposition [3], Wet chemical route [4], Co-precipitation [5], Solvothermal synthesis [6], Hydrothermal process [7], Thermal decomposition method [8], Radio frequency magnetron sputtering technique [9] and Solid state reaction method. Among other established synthesis methods, simple and cost effective routes to synthesize nanocrystalline ZnS by utilization of cheap, nontoxic and environmentally benign precursors are considered as important. Many researchers have studied the electrical properties of ZnS nanoparticles. Solid state reaction method is a very simple and cost effective method compared to other methods.

In the present work, first time, we report a simple solid state reaction method for the Synthesis of different temperatures (250–450 °C) of ZnS nanoparticles with a view to tailoring their photocatalytic applications.

✉ M. Jothibas
jothibas1980@gmail.com

¹ PG & Research Department of Physics, T.B.M.L.College, Porayar, Nagapattinam District, Tamilnadu 609307, India

² Department of Physics, Annamalai University, Annamalai Nagar, Chidambaram, Tamilnadu 608002, India

³ PG & Research Department of Physics, St. Joseph's College of Arts and Science (Autonomous), Cuddalore, Tamilnadu 607001, India

2 Experimental details

2.1 Solid state synthesis of ZnS nanoparticles

In this study, zinc acetate dehydrate ($\text{Zn}(\text{CH}_3\text{COO})_2 \cdot 2\text{H}_2\text{O}$) and thioacetamide (TAA: CH_3CSNH_2) of high purity (procured from E Merck Ltd., Mumbai, India) were used to form ZnS nanoparticles. These chemicals were directly used without special treatment. In typical synthesis, zinc acetate dehydrate and thioacetamide were ground separately by using agate mortar. Then, appropriate amount of these precursors was mixed together and ground thoroughly. Finally, mixed powder was heated in a muffle furnace for 4 h at 250, 300, 350, 400 and 450 °C, respectively. This method was also adapted by Wang and Hong [10] to prepare ZnS nanoparticles.

2.2 Characterization tools

The crystalline phase purity of ZnS was examined by X-ray diffraction (XRD) analysis using SHIMADZU 6000 X-ray diffractometer with $\text{CuK}\alpha$ radiation ($\lambda = 1.5406 \text{ \AA}$) at room temperature. The chemical structure was investigated by SHIMADZU Fourier transform infrared (FTIR) spectrometer in which the IR spectra were recorded by diluting the milled powders in KBr and in the wavelength between 4000 and 400 cm^{-1} . Optical absorption spectra were recorded in the range 200–400 nm using JASCO V-670 spectrophotometer. The photoluminescence (PL) behavior was studied at room temperature by Plorolog 3-HORIBA JOBIN YVON with an excitation wavelength of 325 nm. The surface morphology and elemental composition of the product was demonstrated by SEM with EDX analysis using JEOL JSM 6390.

3 Results and discussion

3.1 Crystallographic analysis

Powder X-ray diffraction patterns of pure ZnS nanoparticles synthesized at different temperatures (250–450 °C) with Miller indices (hkl) showing the crystal family of planes for each diffraction peaks are depicted in Fig. 1. The intense diffraction peaks appearing at about 2θ of 28.42° , 47.69° and 56.41° corresponding with those from (111), (220) and (311) orientations, respectively. This spectra show a strong preferred orientation along (111) direction and comparatively low intensity reflections corresponding to (220) and (311) planes, which is in good agreement with the standard JCPDS (05-0566) values of ZnS compound having face centered cubic (FCC) structure. The XRD

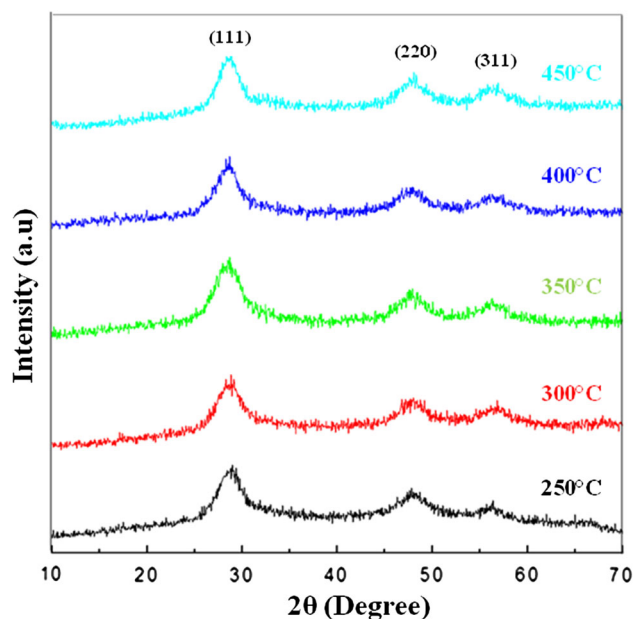


Fig. 1 X-ray diffractograms of cubic ZnS nanoparticles prepared at different temperatures

peaks are significantly broadened because of the very small crystallite sizes [11]. Moreover, no other impurities were detected in the samples, suggesting that pure ZnS were obtained. The crystallite size has been inferred from 2θ and the full width at half maximum (FWHM) of the (111) diffraction peak on the basis of the Scherer's relation,

$$D = \frac{K\lambda}{\beta \cos \theta}$$

where D is the average crystallite size (\AA), K is the shape factor (0.9), λ is the wavelength of X-ray (1.5406 \AA) $\text{Cu K}\alpha$ radiation, θ is the Bragg angle and β is the corrected line broadening of the nanoparticles [12]. Estimated values of the crystallite sizes using this relation are given in Table 1. From this table, we could find that the particle size increases as the temperature of synthesis increases up to 400 °C. At high temperature, perhaps, the reaction gets more energy to grow with larger grain size. This indicates that the size of the crystallites can be adjusted by controlling the temperature of the reaction [13]. The result shows that the average crystallite size of nano ZnS is about 2.84 nm. The lattice parameters 'a', 'b' and 'c' for the cubic structure ($\alpha = \beta = \gamma$, $a = b = c = 90^\circ$) can be determined by the following equation,

$$d = \frac{a}{\sqrt{h^2 + k^2 + l^2}}$$

where h , k and l are the Miller indices of the peak. The microstrain (ϵ) is calculated using the relation,

Table 1 Structural properties of ZnS nanoparticles

Temperature (°C)	Crystallite size D (nm)	Micro strain ε	Lattice constant a (Å)
250	2.55	0.0142	5.4349
300	2.71	0.0133	5.3961
350	2.92	0.0123	5.4342
400	3.06	0.0118	5.4115
450	2.98	0.0121	5.4360

$$\epsilon = \frac{\beta \cos \theta}{4}$$

The calculated lattice parameters for cubic phase of ZnS nanoparticles are presented in Table 1. Thus, it can be revealed that the microstrain showed a decreasing trend with increase in full width half maximum.

3.2 FTIR spectroscopy

FTIR transmission spectra of ZnS nanoparticles synthesized at different temperatures in air for 4 h is shown in Fig. 2. FTIR spectra were recorded in order to identify the functional groups pertaining to ZnS. The spectra show peaks corresponding to ZnS. The ZnS nanoparticles show the characteristics of the formation of high purity products and depict the peaks correspond to ZnS. Several peaks are observed at 3431, 2955, 2340, 2044, 1630, 1399, 796, 617 and 508 cm⁻¹ for the sample. The broad absorption bands at 3431 and 1630 cm⁻¹ are attributed to O–H stretching and bending vibrations of the absorbed water molecules on

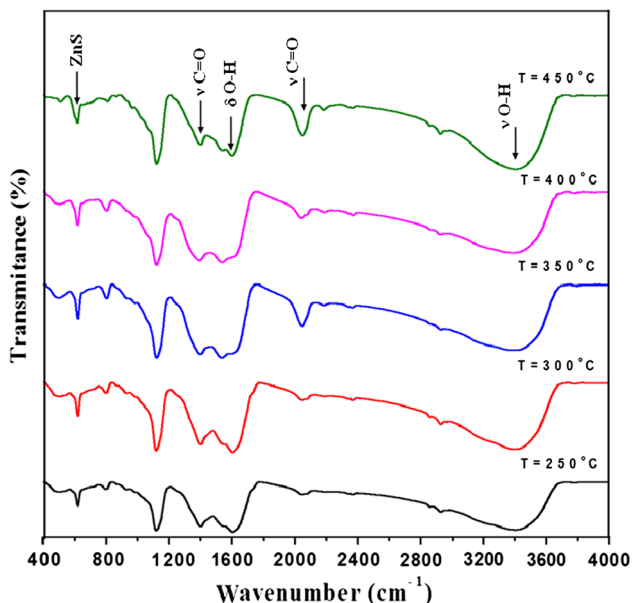


Fig. 2 FTIR spectra of ZnS nanoparticles indicating relative functional groups (*T* temperature)

the surface of nanoparticles, respectively. The bands positioned at around 2955 cm⁻¹ are due to C–H stretching vibration [14]. The peaks at 2340 and 2044 cm⁻¹ are ascribed to the existence of CO₂ molecules. The peak at 1399 cm⁻¹ region could be attributed to carboxyl (C=O) and methylene groups. The peaks appearing at 796, 617 and 508 cm⁻¹ are associated to Zn–S vibration and are characteristic of cubic ZnS [15]. The infrared absorption frequencies and the tentative vibrational assignments of ZnS nanoparticles are depicted in Table 2.

3.3 Optical study

3.3.1 Evaluation of band gap energy

The absorption spectra of the prepared ZnS nanoparticles were illustrated in Fig. 3. The absorption edge at around 320 nm is due to the phase of zinc sulfide. The absorption co-efficient is calculated using the formula,

$$\alpha = \frac{2.303A}{l}$$

where *A* is the absorbance and *l* is the path length. The value of optical band gap is determined from the absorption spectra using the Tauc relation,

$$\alpha h\nu = A(h\nu - E_g)^n$$

where α is the absorption co-efficient, *A* is the constant having separate value for different transitions, *hν* is the

Table 2 Tentative vibrational assignments of ZnS nanoparticles

Wavenumbers (cm ⁻¹)	Assignments
3431	O–H stretching
2955	C–H stretching
2340	CO ₂ molecules
2044	
1630	O–H bending
1399	Carboxyl and methylene groups
796	Zn–S stretching
617	Cubic ZnS
508	

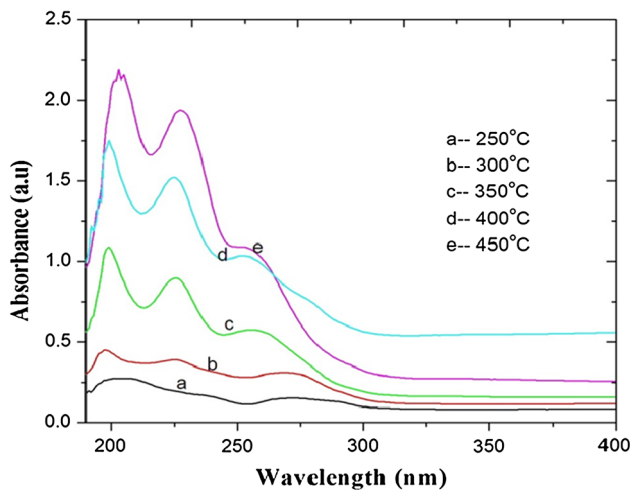


Fig. 3 Optical absorption spectra of ZnS nanoparticles

photon energy and E_g is the band gap energy. The value of n depends upon the nature of transition. The values of n for allowed direct, allowed indirect, forbidden direct and forbidden indirect transition are $1/2$, 2 , $3/2$ and 3 , respectively. The band gap energies are found to be a negative number for $n = 2$, $3/2$ and 3 , and hence the relationship fitting to the ZnS is $n = 1/2$, which confirms the allowed direct transition. Figure 4 shows the curves of $(\alpha h\nu)^2$ versus $h\nu$ for ZnS nanoparticles prepared at different temperatures. The E_g values are obtained by extrapolating the straight line portions of the graph to the X-axis. The measured energy band gaps from these plots are represented in Table 3. From this table, it can be observed that the E_g values varied from 3.69 to 4.24 eV for ZnS nanoparticles prepared at different annealing temperatures. Among the ZnS products, the nanoparticles synthesized at 350 °C exhibits higher band gap energy. So, it has been taken as optimum compound for further investigation. After the electronic absorption process, electrons located in the

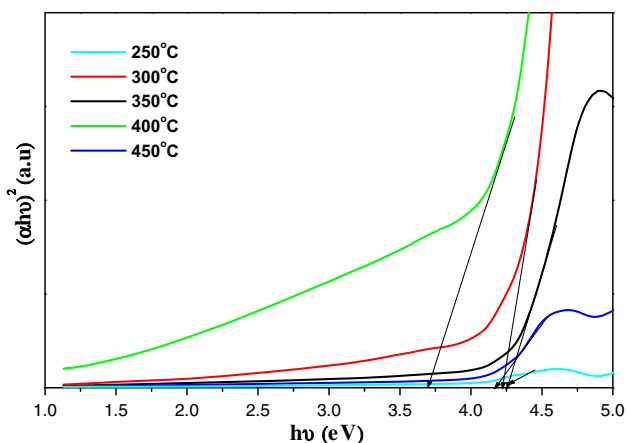


Fig. 4 The plot of $(\alpha h\nu)^2$ versus $h\nu$ for ZnS nanoparticles

Table 3 Calculated band gap energies of ZnS nanoparticles at different temperatures

Temperature (°C)	Band gap energy (eV)
250	4.21
300	4.19
350	4.24
400	3.69
450	4.15

maximum-energy states in the valence band revert to minimum-energy states in the conduction band under the same point in the Brillouin zone [16, 17]. The exponential optical absorption edge and the optical band gap energy are controlled by the degree of structural disorder in the lattice. The decrease in the band gap value can be attributed to defects and local bond distortion as well as intrinsic surface states and, interfaces which yield localized electronic levels within the forbidden band gap [18].

3.3.2 Determination of crystallite size (Brus model)

The band gap energy of ZnS nanoparticles is 4.24 eV, which is higher than the band gap energy of bulk ZnS (3.55 eV) due to the quantum confinement effect. Therefore, the average size of ZnS nanoparticles, in our case, can be estimated by the effective mass theory [19] using relation,

$$E_g(\text{nano}) = E_g(\text{bulk}) + \frac{h^2}{8R^2} \left(\frac{1}{m_e^*} + \frac{1}{m_h^*} \right) - \frac{1.8e^2}{4\pi\epsilon\epsilon_0 R}$$

where $E_g(\text{nano})$ is the energy band of nanoparticles, $E_g(\text{bulk})$ is the energy band of bulk sample, R is the average radius of particles, m_e^* and m_h^* are the effective mass of an electron and a hole, respectively and ϵ stands for the relative dielectric constant ($\epsilon = 8.76$). For ZnS crystal, $m_e^* = 0.23 m_0$ and $m_h^* = 0.34 m_0$ (m_0 is the free electron mass) [20]. The optical measurement usually arrives at a higher “optical band gap” because the direct transition at the fundamental band gap is optically forbidden [21]. However, the particle size of ZnS is calculated from both the absorption spectrum as well as by the analysis of XRD data. The calculated crystallite size of the prepared ZnS (Brus model) is 3.13 nm, where as the crystallite size evaluated from XRD (Scherrer’s method) is around 2.92 nm. This is lower than the value obtained from Brus model; and this may be due to aggregation of nanoparticles. The results show that the synthesized ZnS nanoparticle has excellent optical transparency in the visible region due to the nanosized particles. Which is a key property of transparent oxide materials most widely used in the field of optoelectronic application?

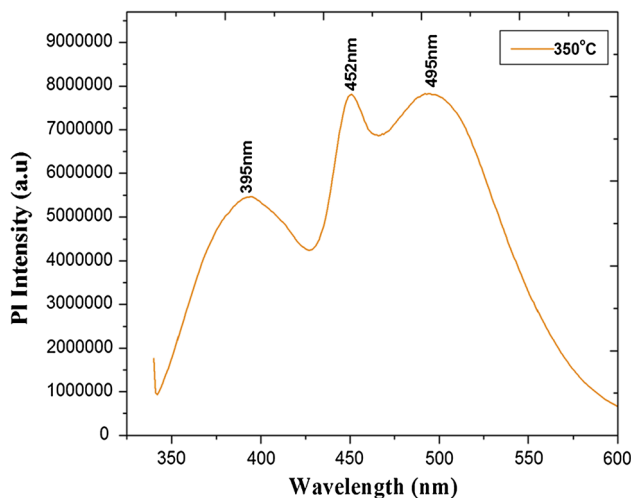


Fig. 5 Photoluminescence emission spectrum of ZnS nanoparticles excited at 325 nm

3.4 Photoluminescence spectroscopy

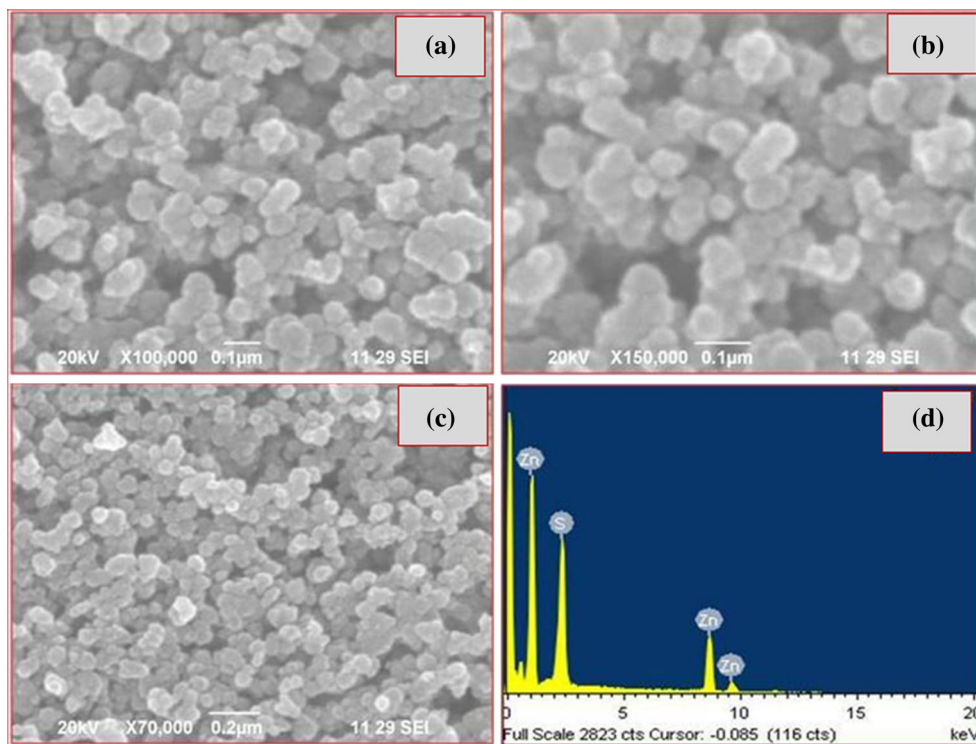
The photoluminescence spectrum of newly synthesized ZnS nanoparticles at 350 °C (represented sample) with an excitation wavelength of 325 nm is shown in Fig. 5. In the PL spectrum, three distinct peaks at 395, 452 and 495 nm are observed. The peak at 395 nm (3.13 eV) in the UV region has been attributed to shallow-trap or defect related

emission of ZnS [22]. The high-intensity blue emission peak at 452 nm (2.74 eV) has been ascribed to the Zn^{2+} vacancy related acceptor [23]. In addition, the emission (green) peak at 495 nm (2.50 eV) can be associated to sulfur vacancy (V_S) [24].

3.5 Morphological characterization

Nanoparticles analysis using SEM supplemented by EDX was carried out for the cubic ZnS to establish the morphology, grain size, shape and to confirm their chemical composition. SEM observed the nano-sized ZnS grains as large surface area with well-defined mesopores and the images are shown in Fig. 6a–c. These micrographs confirm that the nanoparticles are grown in a very high density. Besides, the uniform distribution of particles was found and they consist of either some single particle or a cluster of particles. A closer examination of these pictures reveals a well-defined particle-like morphology, having abundance of spherical shaped particles. The EDX analysis (Fig. 6d) clearly showed that the presence of elements such as Zn and S indicating that the ZnS matrix has composed of zinc and sulfide only. The strong X-ray peaks associated with Zn $\text{K}\alpha$ and S $\text{K}\alpha$ in this spectrum, and from that we noticed that the atomic and weight percentages of Zn and S are 56.59 at.%, 72.66 wt% and 43.41 at.%, 27.34 wt%, respectively.

Fig. 6 a–c SEM micrographs and d EDX spectrum of ZnS nanoparticles annealed at 350 °C



4 Conclusions

The ZnS nanoparticles with different annealing temperatures have been successfully synthesized by solid state reaction method. The XRD results reveal that the particles are polycrystalline with strong preferred grain orientation along (111) plane and exhibit cubic type crystal structure. The optical band gap energy increased with the increase of annealing temperature. The photoluminescence spectra of the ZnS nanoparticles exhibited both UV and visible emissions. The SEM photographs showed densely packed nanoparticles with spherical shape morphology.

References

1. M. Navaneethana, J. Archana, K.D. Nisha, S. Ponnusamy, M. Arivanandhan, Y. Hayakawa, C. Muthamizhchelvan, *Mater. Lett.* **66**, 276–279 (2012)
2. T.Y. Zhou, X. Yuan, J.M. Hong, X.Q. Xin, *Mater. Lett.* **60**, 168–172 (2006)
3. A.K. Kole, S. Gupta, P. Kumbhakar, P.C. Ramamurthy, *Optics Commun.* **313**, 231–237 (2014)
4. M. Navaneethana, J. Archana, K.D. Nisha, Y. Hayakawa, S. Ponnusamy, C. Muthamizhchelvan, *J. Alloys Compd.* **506**, 249–252 (2010)
5. H. Ali, S. Karim, M.A. Rafiq, K. Maaz, A. Rahman, A. Nisar, M. Ahmad, *J. Alloy. Compd.* **612**, 64–68 (2014)
6. L. Dong, Y. Chu, Y. Zhang, *Mater. Lett.* **61**, 4651–4654 (2007)
7. J. Zhaon, R. Liu, *Mater. Lett.* **124**, 239–241 (2014)
8. P.K. Ghosh, U.N. Maiti, S. Jana, K.K. Chattopadhyay, *Appl. Surf. Sci.* **253**, 1544–1550 (2006)
9. W. Zhang, X. Zengn, H. Liu, J. Lu, *J. Lumin.* **134**, 498–503 (2013)
10. L.P. Wang, G.Y. Hong, *Mater. Res. Bull.* **35**, 695–701 (2000)
11. Z.T. Deng, H. Yan, Y. Liu, *Angew. Chem. Int. Ed.* **49**, 8695–8698 (2010)
12. C. Manoharan, M. Jothibas, S. Johnson Jeyakumar, S. Dhana-pandian, *Spectrochim. Acta Part A Mol. Biomol. Spectrosc.* **145**, 47–53 (2015)
13. M.M.H. Farooqi, R.K. Srivastava, *Mater. Sci. Semicond. Process.* **20**, 61–67 (2014)
14. N. Shanmugam, S. Cholan, N. Kannadasan, K. Sathishkumar, G. Viruthagiri, *Solid State Sci.* **28**, 55–60 (2014)
15. G. Murugadoss, M. Rajesh Kumar, *Appl. Nanosci.* **4**, 67–75 (2014)
16. Y.V.B. Santana, C.W. Raubach, M.M. Ferrer, F. La Porta, J.R. Sambrano, V.M. Longo, E.R. Leite, E. Longo, *J. Appl. Phys.* **110**, 123507–123515 (2011)
17. F.A. La Porta, M.M. Ferrer, Y.V.B. Santana, C.W. Raubach, V.M. Longo, J.R. Sambrano, E. Longo, J. Andres, M.S. Li, J.A. Varela, *Curr. Phys. Chem.* **3**, 378–385 (2013)
18. F.A. La Porta, M.M. Ferrer, Y.V.B. de Santana, C.W. Raubach, V.M. Longo, J.R. Sambrano, E. Longo, J. Andres, M.S. Li, J.A. Varela, *J. Alloys Compd.* **556**, 153–159 (2013)
19. L. Brus, *J. Phys. Chem.* **90**, 2555 (1986)
20. K. Arshak, O. Korostynska, J. Henry, *Microelectron. Int.* **21**, 19–27 (2004)
21. A. Walsh, J.L.F. Da Silva, S.H. Wei, C. Korber, A. Klein, L.F.J. Piper, *Phys. Rev. Lett.* **100**, 167402 (2008)
22. N. Karar, F. Singh, B.R. Mehata, *J. Appl. Phys.* **95**, 656 (2004)
23. S.K. Mehta, S. Kumar, S. Chaudhary, K.K. Bhasin, M. Gradzielski, *Nanoscale Res. Lett.* **4**, 17 (2009)
24. N.N. Trung, Q.P. Luu, B.T. Son, L.H. Sinh, J.Y. Bae, *Polym. Compos.* **33**, 1785 (2012)